

Cite this: *RSC Adv.*, 2018, 8, 22177

# A CO<sub>2</sub>-tunable plasmonic nanosensor based on the interfacial assembly of gold nanoparticles on diblock copolymers grafted from gold surfaces†

Huaxiang Chen,<sup>a</sup> Yuliang Wang,<sup>id</sup> Xiaolai Li,<sup>id</sup> Benliang Liang,<sup>a</sup> Shaohua Dong,<sup>\*c</sup> Tingting You<sup>a</sup> and Penggang Yin<sup>id</sup> <sup>\*a</sup>

A general stepwise strategy for the fabrication of CO<sub>2</sub>-tunable plasmonic nanosensors was described for the first time, based on gold surface functionalization by CO<sub>2</sub>-responsive poly(*N,N*-diethylaminoethyl methacrylate) (PDEAEMA) brushes via a surface-initiated atom transfer radical polymerization (SI-ATRP) method, then the extremity of PDEAEMA was functionalized by linking the polyacrylamide (PAAm) brushes via ATRP, where they were assembled with gold nanoparticles (AuNPs) efficiently by altering the deposition time. The swelling–shrinking states of the PDEAEMA brushes can be tuned just by passing CO<sub>2</sub> and N<sub>2</sub> through a solution alternately. The unique plasmonic surface-enhanced Raman scattering (SERS) sensing properties of these stimulative substrates were investigated using 4-mercaptophenol (4MPh) as a molecular probe. When alternating CO<sub>2</sub> and N<sub>2</sub> bubbling in the water solution, the reversible switching of the SERS signals was complete. By *in situ* contact-mode atomic force microscopy, the thickness of the polymer layer was observed to be 26 nm in CO<sub>2</sub> saturated water, and after N<sub>2</sub> bubbling to remove CO<sub>2</sub> it decreased to 15 nm, causing the AuNPs to move near to the gold surface. Meanwhile, the distance between the nearby AuNPs becomes smaller, and the surface coverage ( $\phi$ ) of the AuNPs increased from 27% to 35%. The reported CO<sub>2</sub>-responsive plasmonic nanosensor provided a dynamic SERS platform, with reversible regulation for electromagnetic coupling between the AuNPs and the gold surface, and between nearby AuNPs.

Received 5th April 2018

Accepted 6th June 2018

DOI: 10.1039/c8ra02934b

rsc.li/rsc-advances

## 1. Introduction

Since being discovered by Fleischmann *et al.* in 1974,<sup>1</sup> surface-enhanced Raman scattering (SERS) has garnered vital interest and has become one of the most powerful and sensitive tools for the chemical and biochemical analysis of molecules adsorbed on metallic substrates.<sup>2–7</sup> This technology, with its “fingerprinting” properties and limited influence from water, has a large potential for plasmonic nanosensor applications for characterization and chemical detection.<sup>8</sup> In SERS, high SERS activity is predominantly based on two factors: (i) electromagnetic enhancement, a strong local field enhancement caused by the excitation of a localized surface plasmon (LSP); (ii) chemical

enhancement, observed when a resonant charge transfer occurs between adsorbed molecules and nanoparticles.<sup>9–11</sup>

Currently, one of the key research goals is to fabricate dynamic SERS-active substrates in response to environmental stimuli due to their plasmonic properties and biomedical applications.<sup>12–15</sup> Electric field enhancements, caused by vast “hot spots” within the gap both between two NPs and between NPs and a gold film, can be reversibly altered by changing the environmental conditions, such as temperature and pH. Temperature-responsive gold/PNIPAM/NPs hybrid plasmonic devices were described as a dynamic SERS platform, with thermally switchable electromagnetic coupling between AuNPs and the gold surface, as recently reported by H. Gehan *et al.*<sup>10</sup> However, to the best of our knowledge, gas-responsive dynamic SERS substrates have never been reported so far.

As an important environmental stimulus, carbon dioxide (CO<sub>2</sub>) regulates many organism behaviors, such as finding mates and seeking food.<sup>16,17</sup> In the present study, after the ultrapure water used was saturated with CO<sub>2</sub>, the pH of the solution decreased from 7 to 4.9; while after N<sub>2</sub> bubbling, the initial pH value of 7 was recovered.<sup>18</sup> Brushes of poly(*N,N*-diethylaminoethyl methacrylate) (PDEAEMA) can be switched between swelling and shrinking states just by passing CO<sub>2</sub> and N<sub>2</sub> through the water solution.<sup>19</sup>

<sup>a</sup>Key Laboratory of Bio-inspired Smart Interfacial Science and Technology of Ministry of Education, School of Chemistry, Beihang University, Beijing, 100191, China. E-mail: pgyin@buaa.edu.cn

<sup>b</sup>School of Mechanical Engineering and Automation, Beihang University, Beijing, 100191, China

<sup>c</sup>Pipeline Technology Research Center, China University of Petroleum-Beijing, Beijing, 102249, China. E-mail: shdong@cup.edu.cn

<sup>d</sup>Beijing Advanced Innovation Center for Biomedical Engineering, Beihang University, Beijing, 100083, China

† Electronic supplementary information (ESI) available. See DOI: 10.1039/c8ra02934b

In this work, CO<sub>2</sub>-responsive Au film-PDEAEMA-PAAm-AuNPs hybrid plasmonic nanostructures were fabricated successfully and applied as SERS-active nanosensors. Firstly, PDEAEMA brushes grafted onto a gold surface were obtained *via* ATRP methods. Secondly, the extremity of PDEAEMA was functionalized by linking PAAm brushes *via* ATRP. Lastly, AuNPs were assembled on PAAm layers with different deposition times. On the surface of the samples, AuNPs were fixed efficiently by altering the immersion times. In a CO<sub>2</sub> saturated water solution, the thickness of the polymer layer was as high as 26 nm. After N<sub>2</sub> bubbling, which removes CO<sub>2</sub>, the thickness deceased to 15 nm. Meanwhile, electromagnetic coupling between the AuNPs and the gold surface, or between nearby AuNPs, can be altered reversibly, leading to a reversible change in SERS intensity.

## 2. Materials and methods

### 2.1 Reagents and instruments

Gold coated silicon wafers (<111> oriented, 1000 Å coating, titanium adhesion layer, 0.4 in. × 500 μm) were purchased from Aldrich. 2-(Diethylamino)ethyl methacrylate (DEAEMA, 99% Aldrich) was passed through an activated basic alumina column to remove the inhibitory substances before use. Cu<sup>I</sup>Br (98%), 1,1,4,7,7-pentamethyldi ethylenetriamine (PMDETA, 99%), acrylamide (AAM, 99.9%) and the initiator bis[2-(2-bromoisobutyryloxy)undecyl]disulphide (DTBU) were purchased from Sigma-Aldrich and used as received. 4-Mercaptophenol (4MPH, 99%), methanol (99.8%), ethanol (99.5%) and tetrahydrofuran (99.9%) were purchased from J&K Scientific. All of the deionized water was obtained using a Millipore Direct-Q system.

### 2.2 Preparation of the initiator-modified gold surfaces

Initiator-modified gold surfaces were prepared (Scheme 1, step 1). After being rinsed by tetrahydrofuran, ethanol, water and ethanol, Au-coated silicon wafers were soaked in 1 mM ethanol solution of initiator DTBU, kept immersed for 12 h at 20 °C, then the substrates were washed sequentially with THF and ethanol, and then dried in a stream of nitrogen before use. The initiator-modified gold surfaces (Au film-Br) were immediately

used for polymerization. <sup>1</sup>H-NMR spectra and the chemical structure of DTBU can be seen in Fig. S1.†

### 2.3 ATRP of DEAEMA and AAm on Au film-Br surfaces

Diblock copolymers PDMAEMA-*b*-PAAm grafted from Au film-Br surfaces were synthesized by the ATRP technique.

Firstly, the Br-terminated PDMAEMA brushes on gold films (Au film-PDEAEMA-Br) were prepared (Scheme 1, step 2) according to ref. 19. CuIBr (0.062 g) complexed with PMDETA (0.435 g) as a catalyst, DEAEMA (2.8 g) and MeOH (5 ml) were added in a flask under vigorous stirring, and degassed by three freeze/vacuum/nitrogen cycles. The Au-Br substrates were transferred into the flask and the reaction was continued at 80 °C for 5 h. After polymerization, the Au film-PDEAEMA-Br samples were removed, washed with water and methanol, and then immediately used for the polymerization of PAAm.

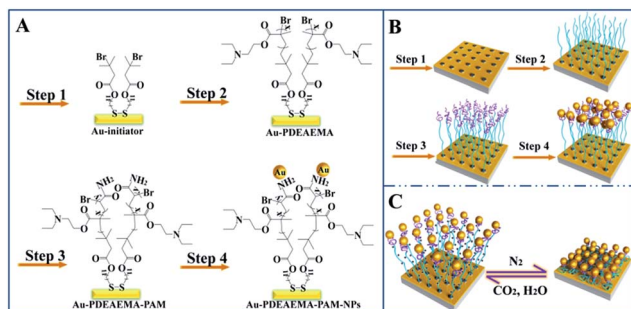
Secondly, PAAm brushes were linked at the end of the PDEAEMA brushes *via* the ATRP method (Scheme 1, step 3). Au film-PDEAEMA-Br samples were transferred to a reaction mixture of PMDETA (0.25 g), Milli-Q water (3 ml), methanol (7 ml), AAm (2.00 g) and CuIBr (0.064 g), and degassed by three freeze/vacuum/nitrogen cycles. The reaction was continued at 25 °C for 10 min, then the Au film-PDEAEMA-PAAm samples were washed sequentially with water and ethanol, and dried in a stream of nitrogen before use.

### 2.4 Au film-PDEAEMA-PAAm assembled with gold nanoparticles

Gold nanoparticles were assembled with amide bonds attached to the PAAm brushes (Scheme 1, part B, step 4). AuNPs with a diameter of 41 nm were synthesized successfully (see Fig. S2†) according to ref. 20. Au film-PDEAEMA-PAAm samples were separately immersed in the AuNP colloidal solution (10 ml) for different periods of time. The prepared Au film-PDEAEMA-PAAm-AuNPs samples were taken out and rinsed with water, then dried with a nitrogen gas stream.

### 2.5 SERS properties of Au film-PDEAEMA-PAAm-AuNPs substrates

The SERS activities of the prepared nanocomposite substrates were tested using 10<sup>−5</sup> M 4MPH as a reporter analyte. Samples were prepared by immersing Au-PDEAEMA-PAAm-AuNPs substrates into 4MPH (10<sup>−5</sup> M, 10 ml) for two hours, then rinsing with ethanol several times to remove the free molecules. The Raman spectra were collected from the SERS samples after



Scheme 1 (A) Stepwise synthetic route of the Au film-PDEAEMA-PAAm-AuNPs substrates. (B) Schematics of the functionalization steps for the prepared Au film-PDEAEMA-PAAm-AuNPs substrates. (C) Schematic of the CO<sub>2</sub>-tunable reversible swelling-shrinking transition.

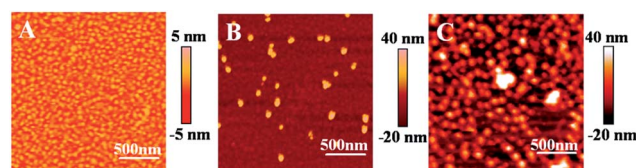
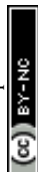


Fig. 1 Tapping mode AFM scans (2 × 2 μm, phase) of the bare Au film (A), Au film-PDMAEMA (B) and Au film-PDEAEMA-PAAm (C) after AuNP deposition for 10 h. Detection in a N<sub>2</sub> saturated water solution.



exposure to CO<sub>2</sub> or upon N<sub>2</sub> bubbling that removes CO<sub>2</sub> in the water solution. The surface-enhanced Raman spectra were measured on an in Via-Reflex micro-Raman system (Renishaw, UK) equipped with a multi-channel charge-coupled device (CCD) detector and a confocal microscope (DM2500 M, Leica) using excitation by a 785 nm laser line.

## 2.6 Characterization

Scanning electron microscopy (SEM) images were recorded by a JEOL JSM7500FA field emission microscope with an accelerating voltage of 5 kV. A JEOL JEM-2100F microscope with an accelerating voltage of 200 kV was selected to produce the transmission electron microscopy (TEM) images. Ultraviolet-visible absorption spectra (UV-vis) were measured on a Shimadzu UV-3150 spectrometer. Fourier transform infrared (FTIR) spectra were collected on a Nicolet iN10 infrared spectrophotometer. An optical contact angle meter (HARKE-CALS) was used to measure the water contact angles with 2  $\mu$ l water droplets under ambient conditions. AFM studies were performed with a Nanoscope III digital instrument microscope (Bruker resolve) in tapping mode to map the film morphology in the water environment.

## 3. Results and discussion

### 3.1 Characterization of the Au film-PDEAEMA-PAAm-AuNPs nanocomposites

The synthesis route of the Au film-PDEAEMA-PAAm-AuNPs nanocomposites is shown in Scheme 1. The successive synthesis of Au film-PDEAEMA and Au film-PDEAEMA-PAAm was confirmed by FTIR spectra. In the FTIR spectrum of the Au film-PDEAEMA surface (Fig. S3A<sup>†</sup>), characteristic peaks of PDEAEMA were observed at 2900–3000 cm<sup>-1</sup> (C–H aliphatic peaks), 1733 cm<sup>-1</sup> (C=O stretching vibration band), 1155–1181 cm<sup>-1</sup> (C–N stretching) and 1067 cm<sup>-1</sup> (N–CH<sub>2</sub> peaks).<sup>21</sup> Moreover, in the FTIR spectrum of the Au film-PDEAEMA-PAAm sample (Fig. S3B<sup>†</sup>), new peaks of 1650 cm<sup>-1</sup> (C=O stretching vibration band of amide group), 3345 cm<sup>-1</sup> (N–H asymmetric stretching) and 3198 cm<sup>-1</sup> (N–H symmetric stretching)<sup>22</sup> confirmed that PAAm brushes were linked at the end of PDEAEMA successfully. The thickness of the PAAm brushes was lower than 5 nm, as reported.<sup>23</sup> After each step in Scheme 1, the change in the contact angle of the prepared material surface also proved the successful preparation of the composite (see Fig. S4<sup>†</sup>).

Next, we discuss the results on the immobilization of AuNPs onto the Au film-PDEAEMA-PAAm surface. In order to confirm that the PAAm layers containing amine functionality can efficiently assemble with AuNPs, we compared the AFM images of Au film-PDEAEMA and Au film-PDEAEMA-PAAm after AuNP deposition for 10 h, as can be seen in Fig. 1. Comparing the two images of (B) and (C), it is evident that the AuNPs were immobilized onto the Au film-PDEAEMA-PAAm surface efficiently.

The loading of AuNPs on the Au film-PDEAEMA-PAAm surface can be controlled by varying the deposition time. It is clearly observed from Fig. 2 that the amount of AuNPs loaded

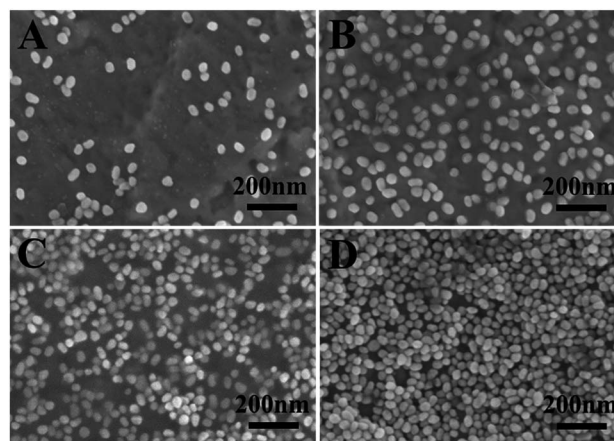


Fig. 2 The SEM images of Au film-PDEAEMA-PAAm-AuNPs at different immersion times of 30 min (A), 5 h (B), 10 h (C) and 20 h (D).

on the surface of the prepared samples increased obviously with an increase in deposition time, and the AuNPs are randomly dispersed on the surface of the samples at deposition times lower than 10 h. However, AuNPs were agglomerated together at a deposition time of 20 h.

### 3.2 CO<sub>2</sub>-tunable SERS efficiency of the prepared samples

To demonstrate the potential CO<sub>2</sub>-response behaviors, samples made of Au-coated Au film-PDEAEMA-PAAm at deposition times of 10 h were evaluated as the optimal SERS active substrates, considering the maximum changes of SERS signal intensity as shown in Fig. 3. SERS signals were collected from the different Au-loading samples in a liquid environment, using 10<sup>-5</sup> M 4MPH as a reporter analyte. A peak at 1080 cm<sup>-1</sup> is assigned to its aromatic ring breathing vibration  $\nu_1$ , and the other peaks at 392, 638, 825, 1009, and 1173 correspond to the ring vibration (see Table S1<sup>†</sup>).<sup>24</sup> In the N<sub>2</sub> saturated water

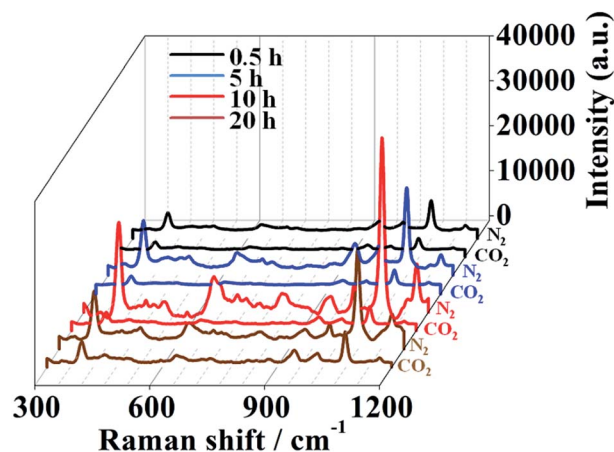


Fig. 3 SERS spectrum of 10<sup>-5</sup> M 4MPH adsorbed on different Au-loading samples, samples in the N<sub>2</sub> saturated water solution for the first detection, then CO<sub>2</sub> bubbling for 30 min for the second detection. The acquisition time was 2 s.



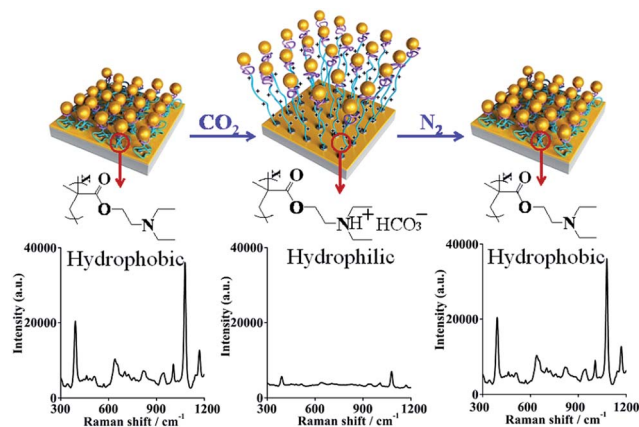


Fig. 4 SERS spectrum of  $10^{-5}$  M 4MPh adsorbed on the optimal sample, samples in the  $N_2$  saturated water solution for the first detection, then  $CO_2$  bubbling for 30 min for the second detection, and  $N_2$  bubbling for 20 min for the third detection. The acquisition time was 2 s.

solution, for all samples, strong SERS signals can be collected, and the strongest SERS signal can be observed at a deposition time of 10 h, as the uniform dispersion of AuNPs provided plenty of plasmonic hotspots. At an immobilization time of 20 h, agglomeration of AuNPs caused the AuNPs to link together, and the quantum tunneling effect greatly reduced the electromagnetic enhancement capability and, as a result, the SERS signal decreased. After  $CO_2$  bubbling for 30 min, the SERS signal decreased obviously, indicating that the number of plasmonic hotspots reduced sharply in this process.

As seen in Fig. 4, upon exposure to the  $CO_2$ -purged aqueous solution for 30 min, the SERS signal showed a drastic decrease as, for the PDEAEMA polymer brushes combined with hydrogen ions, hydrophilic swelling of the PDEAEMA polymer brushes caused the AuNPs to move away from the gold surface, and the distance between the nearby AuNPs increased. After passing  $N_2$  gas for 20 min, the initial SERS signal with strength intensity was recovered as, for the PDEAEMA polymer brushes

dissociated from hydrogen ions, the collapse of the deprotonated PDEAEMA brushes led to the distance between the AuNPs and the gold surface becoming smaller, inducing a huge electric field that became stronger. By regulating the pH from 4 to 7, the SERS signal intensity was significantly enhanced (see Fig. S5†), which confirmed the principle of the response process. The experiments were repeated several times, and the reversible switching of the SERS signal by alternating  $CO_2$  and  $N_2$  bubbling was complete (see Fig. S6†).

AFM measurements were performed to determine the thickness of the copolymer layer under two different conditions in water and the results are summarized in Fig. 5. It was observed that the conformation of the copolymer layer was reversibly changed depending on the bubbling of  $CO_2$  and  $N_2$ . It was revealed that the thickness of the copolymer layer was decreased from 26 to 15 nm after  $N_2$  bubbling, which removes  $CO_2$ . The number of nanoparticles ( $N$ ) per area ( $A$ ) was counted by zooming in on a part of the AFM image, and the surface coverage ( $\phi$ ) was calculated from the following equation:

$$\phi = N\pi d^2/(4A)$$

where  $d$  is the average diameter of the NPs and  $N$  is the number of NPs detected per area  $A$ .<sup>10</sup>

The surface coverage ( $\phi$ ) was increased from 27% to 35% after  $N_2$  bubbling to remove  $CO_2$ , and a red shift can be observed in the UV-vis spectra (as shown in Fig. S7†), indicating that the average distance among the nearby AuNPs decreased obviously. AuNPs moved near to the gold surface and the AuNPs became closer, and these two processes can create vast SERS hotspots for electromagnetic enhancement. The enhancement factor (EF) at  $1080\text{ cm}^{-1}$  of 4MPh adsorbed on the optimal SERS substrates was estimated to be about  $4 \times 10^7$  (in  $N_2$  saturated water) and  $6 \times 10^6$  (in  $CO_2$  saturated water) (detailed calculation process is in ESI†).

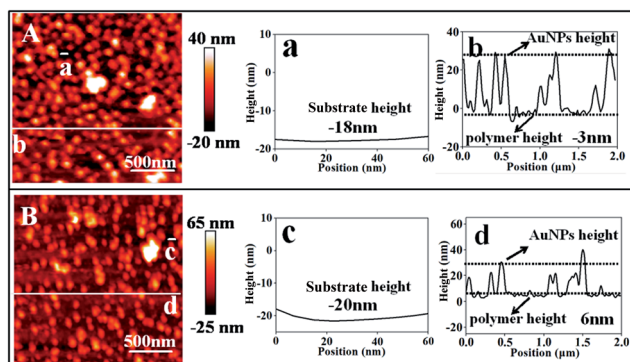


Fig. 5 AFM images of the optimal sample surfaces: (A) in  $N_2$  saturated water; (B) in  $CO_2$  saturated water. Relative heights of the gold surface (a and c) and the polymer film (b and d). The actual height of the polymer film in (A) is calculated as 15 nm (3 nm minus -18 nm), and in (B) it is calculated as 26 nm (6 nm minus -20 nm).

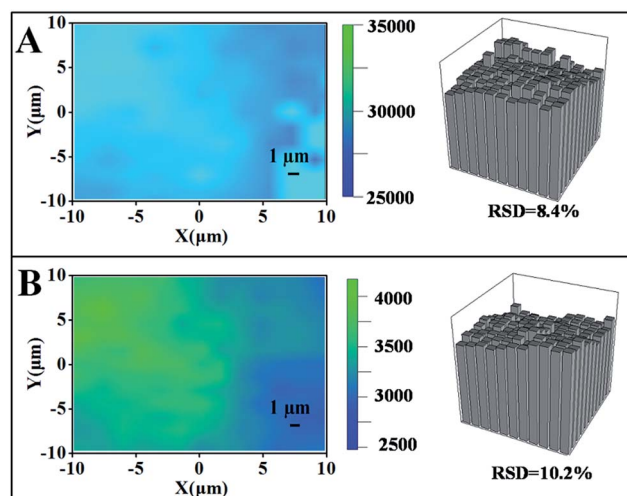


Fig. 6 Raman intensity mapping spectra at  $1080\text{ cm}^{-1}$  of  $10^{-5}$  M 4MPh molecules on a  $20 \times 20\text{ }\mu\text{m}$  surface area of the optimal SERS substrate, detected in  $N_2$  saturated water (A) or in  $CO_2$  saturated water (B). The acquisition time was 2 s.



### 3.3 Homogeneity of the optimal SERS substrates

The homogeneity of a spectral signal through an area is of great importance when considering the practical applications of SERS substrates.<sup>25,26</sup> As shown in Fig. 6, we performed a mapping measurement *via* spot to spot Raman spectroscopy on a 20  $\mu\text{m} \times 20 \mu\text{m}$  area of the optimal samples with a step size of 1  $\mu\text{m}$  to evaluate the homogeneity of the SERS signals, detected after exposure to  $\text{CO}_2$  or upon  $\text{N}_2$  bubbling that removes  $\text{CO}_2$  in the water solution. The relative standard deviation (RSD) of a Raman intensity of 1080  $\text{cm}^{-1}$  was calculated to be 8.4% in the state of collapse (Fig. 6A). After exposure to  $\text{CO}_2$ , the PDEAEMA brushes swell, causing the SERS intensity to decreased sharply with an RSD of 10.2% (Fig. 6B), indicating the stability and uniformity of SERS substrates in large areas under the  $\text{CO}_2/\text{N}_2$  response process.

## 4. Conclusions

In summary, a novel  $\text{CO}_2$ -responsive plasmonic nanosensor was successfully fabricated by a general stepwise strategy: PDEAEMA brushes with  $\text{CO}_2$ -response properties were synthesized *via* ATRP grafted from gold surfaces, after which PAAM brushes were linked at the end of the PDEAEMA brushes, and AuNPs were fixed to the PAAM brushes with high final efficiency. The prepared samples at deposition times of 10 h were selected as the optimal SERS substrates.

After alternating  $\text{CO}_2$  and  $\text{N}_2$  bubbling in the water solution, the reversible switching of the SERS signals was complete, using 4MPh ( $10^{-5}\text{M}$ ) as the target. Changes in polymer layer thickness were observed by AFM: the thickness was 26 nm in  $\text{CO}_2$  saturated water, and decreased to 15 nm after  $\text{N}_2$  bubbling to remove  $\text{CO}_2$ . Meanwhile, AuNPs were near to the gold surface, and the distance between the nearby AuNPs became closer, leading to vast hotspots which can give rise to electromagnetic enhancement obviously. The RSD of the optimal SERS substrates was calculated to be 10.2% in  $\text{CO}_2$  saturated water and 8.4% in  $\text{N}_2$  saturated water, indicating that the optimal SERS nanosensor was stable in a large area under the  $\text{CO}_2/\text{N}_2$  response process.

## Conflicts of interest

There are no conflicts of interest to declare.

## Acknowledgements

This work was supported by the National Natural Science Foundation of China (51572009) and the National Key R&D Program of China (2017YFC0805800).

## References

- 1 M. Fleischmann, P. J. Hendra and A. J. Mcquillan, *Chem. Phys. Lett.*, 1974, **26**(2), 163–166.
- 2 K. G. Li, Y. Wang, K. Jiang, Y. Ren, Y. Q. Dai, Y. H. Lu and P. Wang, *Nanotechnology*, 2016, **27**(49), 495402.
- 3 Y. W. Wang, B. Yan and L. X. Chen, *Chem. Rev.*, 2013, **113**(3), 1391–1428.
- 4 A. Campion, J. E. I. Iii, C. M. Child and M. Foster, *J. Am. Chem. Soc.*, 1995, **117**(47), 11807–11808.
- 5 J. Xie, Q. Zhang, J. Y. Lee and D. I. C. Wang, *ACS Nano*, 2008, **2**(12), 2473–2480.
- 6 X. Li, G. Chen, L. Yang, Z. Jin and J. Liu, *Adv. Funct. Mater.*, 2010, **20**(17), 2815–2824.
- 7 S. E. Deprimo, J. Cao, M. N. Hersh and J. R. Stringer, *J. Phys. Chem. C*, 2011, **115**(36), 17829–17835.
- 8 S. Gupta, M. Agrawal, M. Conrad, N. A. Hutter, P. Olk, F. Simon, L. M. Eng, M. Stamm and R. Jordan, *Adv. Funct. Mater.*, 2010, **20**(11), 1756–1761.
- 9 P. G. Yin, Y. Chen, L. Jiang, T. T. You, X. Y. Lu, L. Guo and S. H. Yang, *Macromol. Rapid Commun.*, 2011, **32**(13), 1000–1006.
- 10 H. Gehan, L. Fillaud, M. M. Chehimi, J. Aubard, A. Hohenau, N. Felidj and C. Mangeney, *ACS Nano*, 2010, **4**(11), 6491–6500.
- 11 L. Jensen, C. M. Aikens and G. C. Schatz, *Chem. Soc. Rev.*, 2008, **37**(5), 1061–1073.
- 12 K. Qian, L. Yang, Z. Li and J. Liu, *J. Raman Spectrosc.*, 2013, **44**(1), 21–28.
- 13 M. Lin, Y. Wang, X. Sun, W. Wang and L. Chen, *ACS Appl. Mater. Interfaces*, 2015, **7**(14), 7516–7525.
- 14 Y. Zhang, H. Hong, D. V. Myklejord and W. Cai, *Small*, 2011, **7**(23), 3261–3269.
- 15 X. Y. Liu, X. Q. Wang, L. S. Zha, D. L. Lin, J. M. Yang, J. F. Zhou and L. Zhang, *J. Mater. Chem. C*, 2014, **2**(35), 7326–7335.
- 16 Y. L. Xu, X. Sui, S. Guan, J. Zhai and L. Gao, *Adv. Mater.*, 2015, **27**(11), 1851–1855.
- 17 G. S. B. Suh, A. M. Wong, A. C. Hergarden, J. W. Wang, A. F. Simon, S. Benzer, R. Axel and D. J. Anderson, *Nature*, 2004, **431**(7010), 854–859.
- 18 J. T. Sun, C. Y. Hong and C. Y. Pan, *J. Phys. Chem. C*, 2010, **114**(29), 12481–12486.
- 19 S. Kumar, X. Tong, Y. L. Dory, M. Lepage and Y. Zhao, *Chem. Commun.*, 2013, **49**(1), 90–92.
- 20 G. Frens, *Nat. Phys. Sci.*, 1973, **241**(105), 20–22.
- 21 D. Q. Wang, J. J. Tan, H. L. Kang, L. Ma, X. Jin, R. G. Liu and Y. Huang, *Carbohydr. Polym.*, 2011, **84**(1), 195–202.
- 22 X. X. Kong, T. Kawai, J. Abe and T. Iyoda, *Macromolecules*, 2001, **34**(6), 1837–1844.
- 23 Q. Liu, A. Singh, R. Lalani and L. Liu, *Biomacromolecules*, 2012, **13**(4), 1086–1092.
- 24 C. Y. Song, J. L. Abell, Y. P. He, S. H. Murph, Y. P. Cui and Y. P. Zhao, *J. Mater. Chem. C*, 2011, **22**(3), 1150–1159.
- 25 B. B. Ma, P. Li, L. B. Yang and J. H. Liu, *Talanta*, 2015, **141**, 1–7.
- 26 C. Farcau and S. Astilean, *J. Phys. Chem. C*, 2010, **114**(27), 11717–11722.

